JOINT INSTITUTE FOR NUCLEAR RESEARCH
Veksler and Baldin Laboratory of High Energy Physics

FINAL REPORT ON THE START PROGRAMME

First steps in the Short-Range Correlations analysis of physics data collected in 2022 with a 45 GeV/c carbon beam

Student:
Stepan Cherepanov, Russia
Moscow State University

Supervisor:
Ph.D. Maria Patsyuk

Participation period:
July 06 - August 30

Dubna
2025

Abstract

This report summarizes the first glance at the physics analysis aiming at studying of events containing hard quasielastic knockout of Short-Range Correlated pairs of nucleons from the carbon-12 nucleus in the reaction $^{12}C(p, 2p)^{10}B/^{10}Be$ under conditions, when the knocked-out and scattered protons are detected at 30 degrees with respect to the beam direction.The carbon-12 beam was produced and accelerated in Booster and Nuclotron of the NICA mega-science facility and scattered on a liquid hydrogen target at the modified BM@N experimental setup.

Contents

1 Introduction

The BM@N experiment is the first fixed-target experiment at the NICA accelerator megascience complex under construction at JINR (Dubna, Russia). The experiment investigates dense baryonic matter using heavy-ion beams. In 2017, the physics program of BM@N was expanded to study short-range correlations (SRC) in carbon nuclei in the reaction $^{12}\mathrm{C}(p, 2p)X$, where $X = {}^{11}\mathrm{B}$, $^{10}\mathrm{B}$, $^{10}\mathrm{Be}$. SRC are short-lived fluctuations of strongly interacting nucleon pairs in which the nucleons are separated by distances comparable to the radius of a single nucleon and carry momenta exceeding those of nucleons in the shell model of the nucleus. The theoretical framework on SRC is currently developed well enough to allow quantitative comparisons between calculations and experiment. The quantity and quality of available experimental data make it possible to obtain numerical estimates of the parameters entering theoretical calculations.

The first BM@N experiment in 2018 showed [1] that when the $^{11}\mathrm{B}$ nucleus is detected, the nucleon knockout proceeds through a "transparent" carbon nucleus, implying suppression of interactions in the initial and final states. Twenty-five events of SRC-pair knockout were recorded, with properties consistent with results obtained on electron beams. In 2022, the experiments continued with an improved detector system that included a hadron calorimeter to better separate proton signals from background pions, as well as upgraded scintillation counters. The introduction of a laser system made it possible to calibrate all scintillation detectors simultaneously in the absence of beam. The improved data-acquisition and analysis methods, together with a larger event sample than in the 2018 run, expand the capability to detect SRC pairs.

2 Experimental Setup

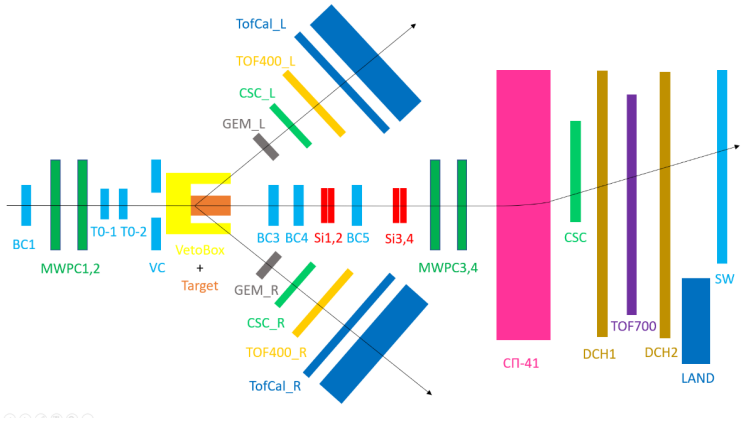

Figure 1: Schematic of the experimental setup. Not to scale.

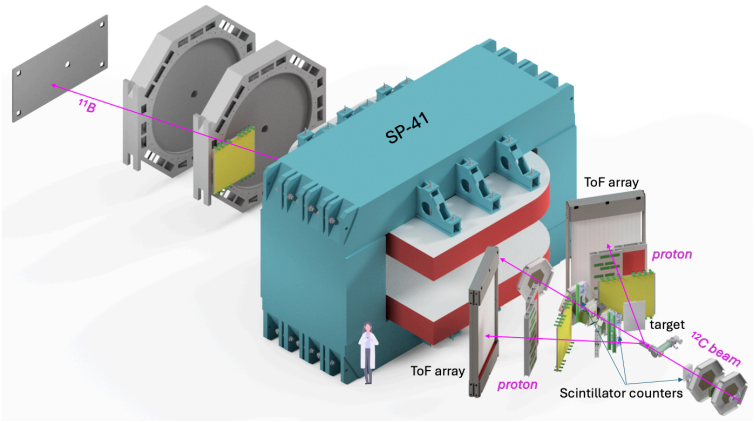

Figure 2: A model view of the experimental setup.

The first and second JINR SRC measurement in inverse kinematics were performed at the BM@N spectrometer with a 48 GeV/c and 44.4 GeV/c momentum carbon beam from the Nuclotron accelerator incident on a proton target [2] in 2018 and 2022, respectively. The baseline configuration of the BM@N setup was modified with the two-arm spectrometer for registration of the scattered and knocked-out protons at an angle of 30° with respect to the beam, which corresponds to back-to-back elastic (pp, pp) scattering in the center-of-mass system. The auto-model behavior [3] of the elastic (pp, pp) cross section near 90° was used to increase

the probability of interactions with high-momentum nuclear protons. The details and the results of the 2018 pilot measurement can be found in [1]. Inspired by the first successful measurement, which served as a proof of concept and allowed accessing ground state properties of ^{12}C in a quasi-free unperturbed single-step reaction ^{12}C (p, 2p) ^{11}B as well as measuring properties of SRC pairs, the second measurement was conducted in 2022. It aimed at measuring the absolute cross sections, quenching, and attenuation at high momentum transfer for the cases of quasi-elastic single proton knockout reaction. And for the SRC studies the main objectives were to achieve higher statistics, detect the recoil partner, and perform multi-fragment reconstruction with the idea to study fragmentation patterns and get a clue on the production mechanism of SRC pairs.

To achieve these goals, several aspects of the experimental setup were improved compared to 2018. The schematic view and 3D model of the experimental setup in 2022 are shown in Fig. 1 and 2 correspondingly. Two new start time scintillator beam counters and three scintillator counters for charge measurements were designed and produced to achieve a better time and amplitude resolutions. Each counter was read out by two PMTs, and the light signal was transported from the scintillator to the PMT window by a Plexiglas light guide (compared to a single PMT for each counter and air light guides in 2018). The new compact cryogenic liquid hydrogen target [4] was designed, developed, and manufactured at JINR. Two pairs of double-sided Si detectors, where each second detector was rotated by 90 degrees with respect to the beam direction, were used for coordinate measurements of the fragments downstream the target. The two-arm spectrometer was improved with new detectors compared to 2018. Each arm contained a GEM (Gas Electron Multiplier) [5] and a CSC (Cathode-Strip Chamber) coordinate planes as well as a time-of-flight TOF400 detector based on MRPC (Multi-gap Resistive Plate Chambers) technology. The new large-area Tof-Calorimeter with the width of 1.5 m and height of 2 m was assembled at JINR and located at each arm. Tof-Calorimeter consisted of a scintillator array providing timing information and three layers of LAND [6] modules providing statistical proton/pion separation. Downstream the analyzing magnet a CSC was added for tracking of light fragments with large turn-

ing angles. The scintillator wall provided charge information for each fragment in the final state. A new laser calibration system with optical fibers going to all scintillator detectors was used to perform time calibration without beam. The main physics trigger was formed based on the signals from the scintillator beam counters and the scintillator layer of the Tof-Calorimeter on both arms.

3 SRC analysis

Before detailing the SRC selections, we summarize the reconstruction and preselection applied to the data. A full analysis of all individual detector subsystems was performed, tracks of the two-arm spectrometer were formed, and the interaction vertex was determined in each event. The track of the ion entering the target and the tracks of forward fragments along the beam were reconstructed, and particle identification together with momentum measurement was carried out using straight track segments of the fragments before and after the analyzing magnet. From the entire collected data set, events were retained in which the residue fragment is identified as a ^{10}B, ^{10}Be, or ^{11}B ion.

The analysis presented here is carried out on a subset of events that satisfy the following criteria: one track reconstructed with the silicon tracking detectors and the MWPC detectors; the condition on particle β in the range $0 \leq \beta \leq 1.5$; and exactly one track in each arm of the two-arm detector.

Subsequent selection was performed on a data tree named:
PhysicsTree_7_7_3500_4999_HeavyFrag_RotLeft0_2deg_JuneFilesFrag.root.

3.1 Single proton knockout

We identify exclusive $^{12}\mathrm{C}(p,2p)^{11}\mathrm{B}$ events by requiring the detection of a ^{11}B fragment in coincidence with two charged-particle tracks. Energy and momentum conservation for this reaction reads:

$$\bar{p}_{12\mathrm{C}} + \bar{p}_{tg} = \bar{p}_1 + \bar{p}_2 + \bar{p}_{11\mathrm{B}}, \tag{1}$$

where $\bar{p}_{12\mathrm{C}} = \left(\sqrt{\mathbf{p}_{12\mathrm{C}}^2 + m_{12\mathrm{C}}^2},\ 0,\ 0,\ p_{12\mathrm{C}}\right)$ and $\bar{p}_{tg} = (m_p, 0, 0, 0)$ are respectively the incident beam-ion and target proton four-momentum vectors. $\bar{p}_1$, $\bar{p}_2$, and $\bar{p}_{11\mathrm{B}}$ are the four-momentum vectors of the detected protons and ^{11}B fragment. Assuming QE scattering off a nucleon which is moving in a mean-field potential, we can approximate $\bar{p}_{12\mathrm{C}} = \bar{p}_i + \bar{p}_{11\mathrm{B}}$, where $\bar{p}_i$ is the initial proton four-momentum inside the ^{12}C ion. Substituting into Eq. (1) we obtain:

$$\bar{p}_i \approx \bar{p}_{\mathrm{miss}} \equiv \bar{p}_1 + \bar{p}_2 - \bar{p}_{tg}, \tag{2}$$

where $\bar{p}_{\mathrm{miss}}$ is the measured missing four-momentum of the reaction and is only equal to $\bar{p}_i$ in the case of unperturbed (no ISI/FSI) QE scattering. Throughout the text, the missing-momentum vector is shown and discussed after being boosted from the lab frame to the incident ^{12}C rest frame.

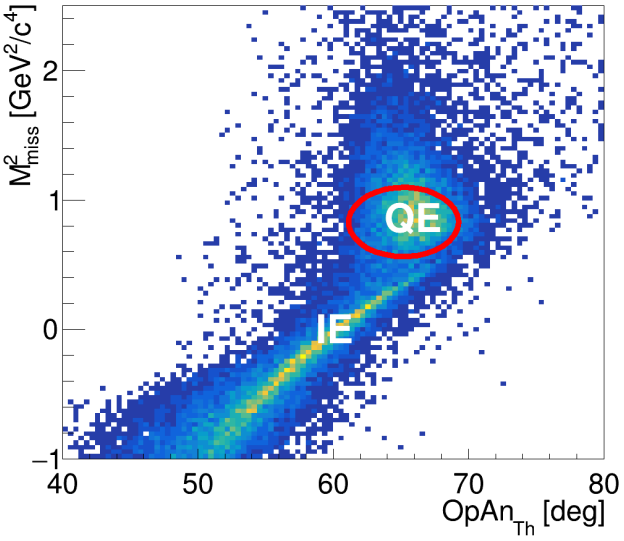

Figure 3: **Quasi-Free Scattering distribution**. The correlation between the measured missing-mass and the measured lab-frame two-proton in-plane opening angle $(\theta_1 + \theta_2)$. Distributions are shown for exclusive $^{12}C(p, 2p)^{11}B$ events.The QE events were selected according to an elliptical cut shown in red. The inelastic (IE) peak region is also marked.The selection criteria include beta cut for the two protons in the arms, the vertex cut in X,Y,Z axes, and the minimal |t,u| cut (see Addendum).

Figure 3 shows correlation between the measured missing mass squared it is the square of four vectors of $\bar{p}_{\text{miss}}$ in the ^{12}C rest frame) and the lab-frame two-proton in-plane opening angle, $\theta_1 + \theta_2$, for exclusive $^{12}\text{C}(p, 2p)^{11}\text{B}$ events. The distribution shows two distinct regions: (A) low missing energy and large in-plane opening angles that correspond to QE (quasi-elastic area) scattering, and (B) high missing energy and small in-plane opening angles that correspond to IE scattering (inelastic area).

To suppress the contribution of quasi-elastic (QE) events in the selection of SRC pairs, we introduce on the $(\theta_1 + \theta_2,\ m^2_{\text{miss}})$ plane an elliptical veto region defined by (see Fig. 2, red contour)

$$\left(\frac{\theta - \overline{\theta}}{a_\theta}\right)^2 + \left(\frac{m^2_{\text{miss}} - \overline{m^2}}{a_{m^2}}\right)^2 \leq 1,$$

where the ellipse center is $\overline{\theta} = 65.6^\circ$, $\overline{m^2} = 0.896\ \text{GeV}^2/c^4$. The angular semi-axis is taken as $a_\theta = n_\theta\, \sigma_\theta$ with $\sigma_\theta = 2.22^\circ$, $n_\theta = 2$, hence $a_\theta = 4.44^\circ$. The m^2_{miss} semi-axis is taken as $a_{m^2} = n_{m^2}\, \sigma_{m^2}$ with $\sigma_{m^2} = 0.232\ \text{GeV}^2/c^4$, $n_{m^2} = 1.1$, hence $a_{m^2} = 0.255\ \text{GeV}^2/c^4$.

3.2 Selecting high-momentum SRC events

We study SRC events by focusing on $^{12}\text{C}(p, 2p)^{10}\text{B}$ and $^{12}\text{C}(p, 2p)^{10}\text{Be}$ events. Most of the selection is based on establishing cut-offs for momenta and missing masses for nucleons flying out of the nucleus on collision with a proton. The four momenta of these particles are determined by the formulas, see also Fig. 4:

$$p_{miss} = p_1 + p_2 - p_{\text{tg}} \tag{3}$$

$$p_{\text{rec}} = p_{^{12}\text{C}} + p_{\text{tg}} - p_1 - p_2 - p_{A-2} \tag{4}$$

We start with the two-proton detection imposing the vertex, β and min(|t|,|u|)

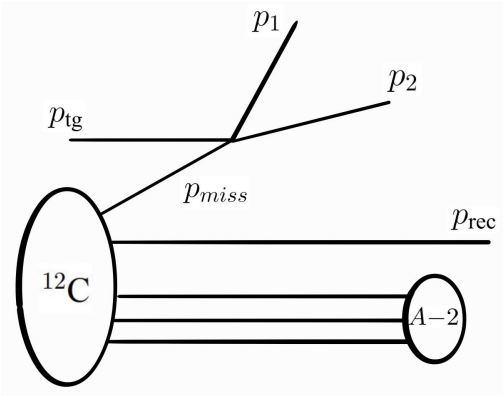

Figure 4: The diagram of the hard quasi-free knockout of an SRC pair out of 12-C nucleus.

cuts, see Addendum. Furthermore, to limit the influence of inelastic scattering, we impose a restriction on the missing mass in the square 0.5 GeV$^2/c^4 < M^2_{\rm miss} < 1.5$ GeV$^2/c^4$ in the reaction ^{12}C$(p,2p)^{11}$B , as shown in Fig. 5, where $M^2_{\rm miss} = E^2_{\rm miss} - \mathbf{p}^2_{\rm miss}$.

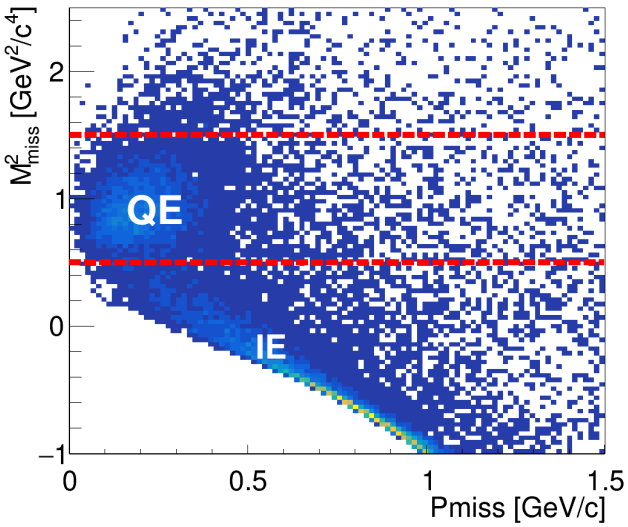

Figure 5: Distribution of events in the $p_{\rm miss}$–$M^2_{\rm miss}$ plane. The quasi-elastic (QE) events are concentrated around $M^2_{\rm miss} \simeq 1$ GeV$^2/c^4$, while inelastic (IE) contributions dominate at lower $M^2_{\rm miss}$. To suppress inelastic scattering and background events, the cut $0.5 < M^2_{\rm miss} < 1.5$ GeV$^2/c^4$ (red lines) is applied.

At the moment, for the current analysis, we do not have a simulation, but

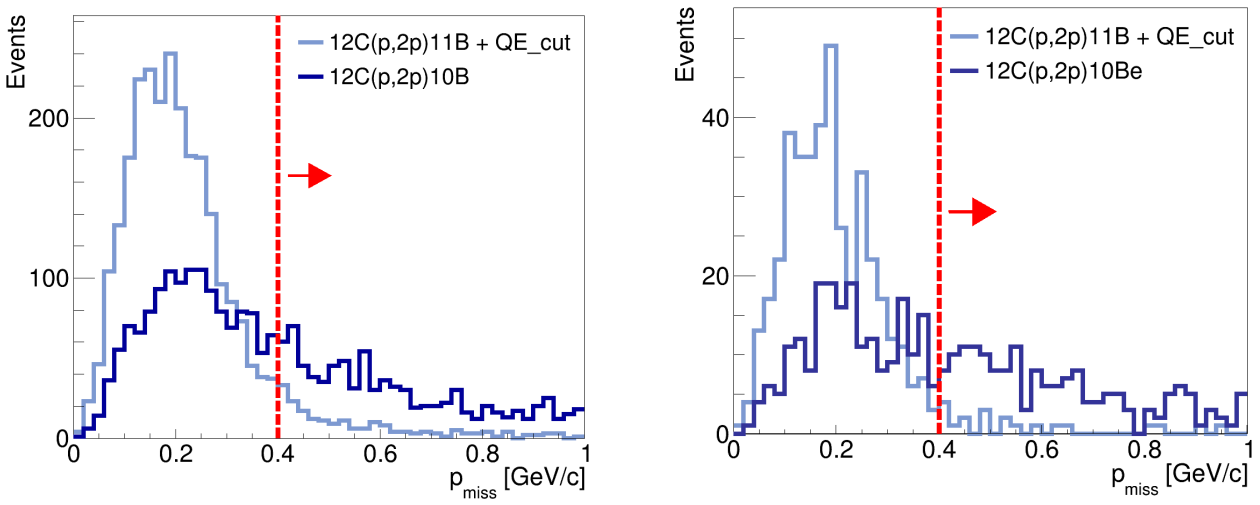

Figure 6: Missing momentum distributions for $^{12}\mathrm{C}(p,2p)^{11}\mathrm{B}$ (with QE cut) in light blue and $^{12}\mathrm{C}(p,2p)^{10}\mathrm{B}$ in dark blue events (left), $^{12}\mathrm{C}(p,2p)^{10}\mathrm{Be}$ events in light blue (right). The vertical red line at $|p_{\mathrm{miss}}| = 400$ MeV$/c$ indicates the applied cut used to suppress the mean-field contributions.

we can assume that the QE region can be described by a mean-field potential and compare the QE behavior to the potential SRC behavior based on data only. We show distributions normalized to the same number of events for SRC selection.

While ^{10}B and ^{10}Be fragments can be produced in SRC breakup reaction, they can also be produced following $(p,2p)$ interactions involving mean-field nucleons. $\sim 10\%$ of the measured inclusive mean-field $^{12}\mathrm{C}(p,2p)$ QE events produce excited ^{11}B fragment that decay to ^{10}B and ^{10}Be via nucleon emission. These processes can be suppressed by requiring $|p_{\mathrm{miss}}| > 400$ MeV$/c$, which selects protons with initial momenta that is well above the nuclear Fermi level where SRCs predominate over mean-field nucleons [7], see Fig. 6.

To suppress the remaining contribution from nucleons described by the mean field, a cutoff must be imposed on M^2_{rec}: $0 < M^2_{\mathrm{rec}} < 1.1$ GeV$^2/c^4$, where $M^2_{\mathrm{rec}} = E^2_{\mathrm{rec}} - \mathbf{p}^2_{\mathrm{rec}}$. Figure 7 shows that this condition suppresses almost all events from mean field nucleons.

For additional comparison, Fig. 8 and 9 show graphs depicting the results of SRC pair selection in the $^{12}\mathrm{C}(p,2p)^{10}\mathrm{B}$ and $^{12}\mathrm{C}(p,2p)^{10}\mathrm{Be}$ reactions and nu-

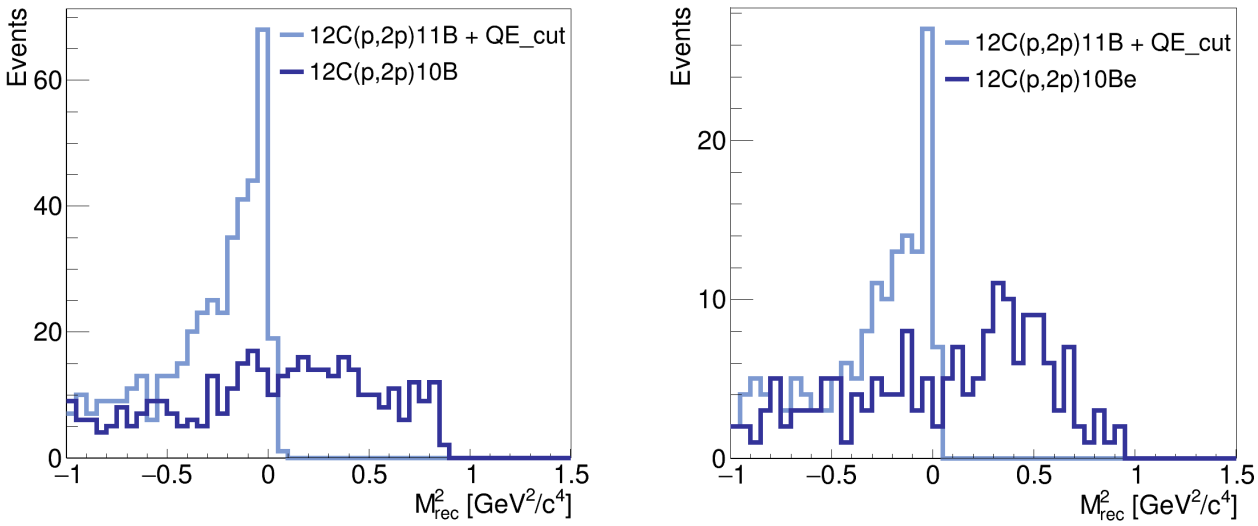

Figure 7: Distributions of M^2_{rec} for $^{12}\text{C}(p,2p)^{10}\text{B}$ (left) and $^{12}\text{C}(p,2p)^{10}\text{Be}$ (right) events in light blue compared with $^{12}\text{C}(p,2p)^{11}\text{B}$ events in dark blue (with QE cut). The applied cut $0 < M^2_{\text{rec}} < 1.1$ GeV$^2/c^4$ suppresses almost all contributions the mean-field nucleons.

cleons described by the mean field in the $^{12}\text{C}(p,2p)^{11}\text{B}$ with the addition of a QE cut. These distributions allow us to check how strongly the applied constraints suppress the contribution of the quasi-elastic background and to compare the kinematic observables. In particular, the variables $\alpha_m = (e_{miss} - p_{miss,z})/m_N$, M^2_{miss}, $E_{\text{miss}} = m_N - e_{miss}$ and the opening angle $\theta_{\text{p}_1} + \theta_{\text{p}_2}$, where α_m is the light cone variable, e_{miss} is the energy component of the four momentum p_{miss}, m_N is the nucleon mass.

Furthermore, the observed distributions suggest that an additional selection criterion $\alpha_m < 0.85$ can be introduced, which is shown by the red line in the distribution graphs for alpha in Figures 8 and 9. This requirement provides additional suppression of residual quasi-elastic events that may pass through the selection described above, thereby ensuring that genuine SRC pairs, rather than mean field contributions, predominate in the selected sample.

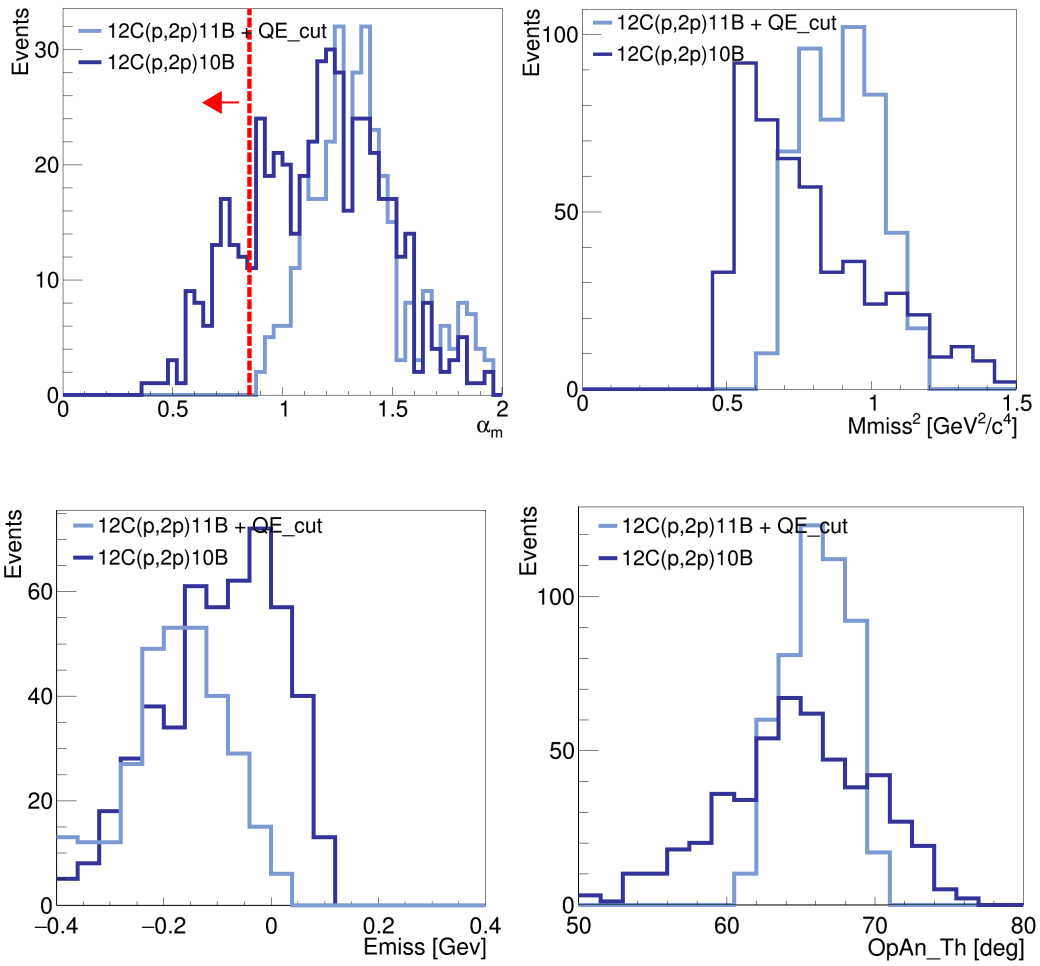

Figure 8: Distributions of α_m, M^2_{miss}, E_{miss} and θ_{pp} for $^{12}\text{C}(p,2p)^{10}\text{B}$ in light blue compared with the reference $^{12}\text{C}(p,2p)^{11}\text{B}$ sample in dark blue (with QE cut).

3.3 Results

In the current work the first glance at the selection of SRC events from the 2022 data was done, showing that a set of cuts can be elaborated in order to cleanly separate SRC events from QE events. The preliminary selection of events can be seen in Table 1 .

After applying a sequence of cuts based on the reaction vertex position, β selection, min(|t|,|u|), M^2_{miss}, M^2_{rec}, missing momentum, and alpha cuts, we obtain a sample of SRC candidate events. As shown in Table 1, the number of selected pn-knockout pairs in the reaction $^{12}\text{C}(p,2p)^{10}\text{B}$ is approximately 92, while the number

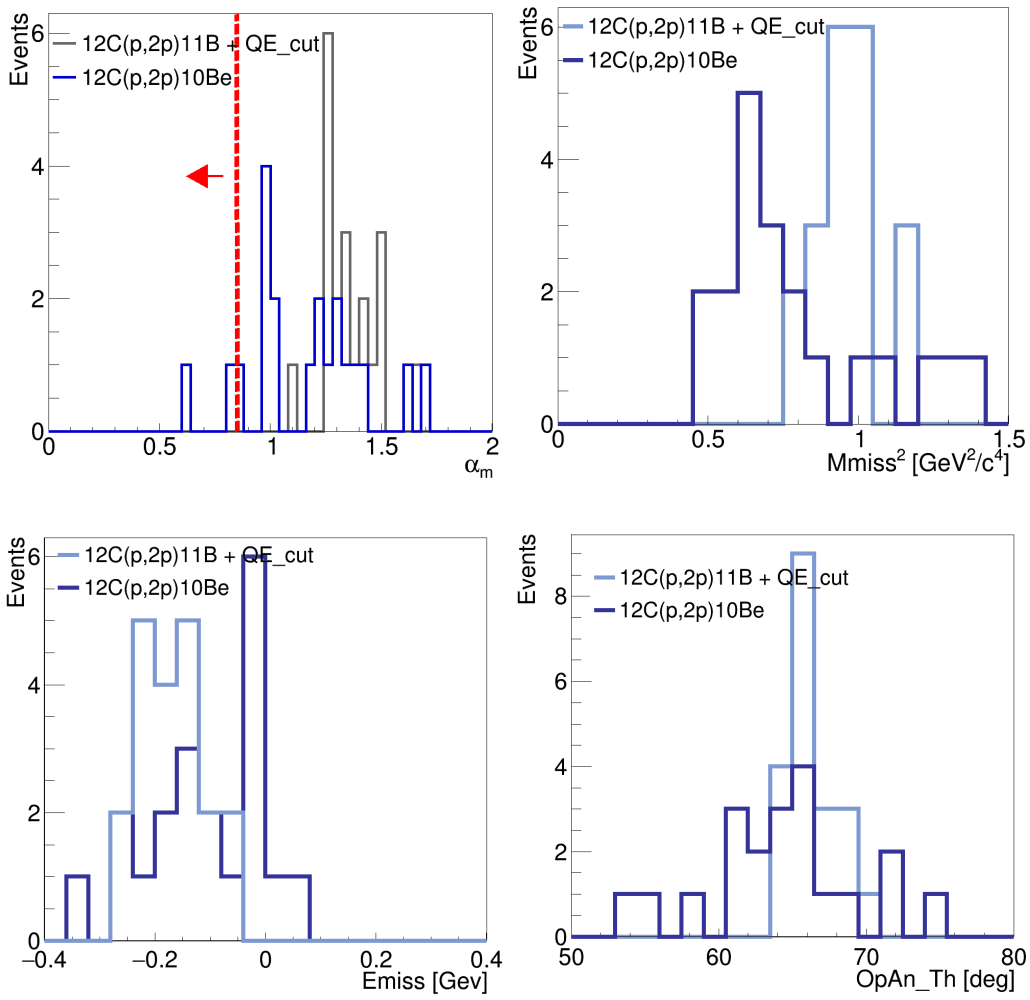

Figure 9: Distributions of α_m, M^2_{miss}, E_{miss} and θ_{pp} for $^{12}\text{C}(p,2p)^{10}\text{Be}$ in light blue compared with the reference $^{12}\text{C}(p,2p)^{11}\text{B}$ sample in dark blue (with QE cut).

of pp-knockout pairs in the reaction $^{12}\text{C}(p,2p)^{10}\text{Be}$ is about 14.

Next we examine the angular correlations between the nucleons in the pair and between the pair and the ^{10}B and ^{10}Be fragment. Figures 10a and 10c show the distribution of the cosine of the angle between the missing momentum and the reconstructed undetected recoil neutron momentum for the reactions $^{12}\text{C}(p,2p)^{10}\text{B}$ and $^{12}\text{C}(p,2p)^{10}\text{Be}$, respectively. A clear back-to-back correlation is observed, as expected for strongly-correlated nucleon pairs.

Finally, we consider the factorization of measured SRC pairs from the residual nuclear system. The strong two-body interaction between nucleons in a pair

Selection step	^{12}C$(p,2p)^{10}$B (pn knockout)	^{12}C$(p,2p)^{10}$Be (pp knockout)
(p,2p) tagging, $b_{L(R)} < 0.98$, vertex cut	34575	6039
$min(\|t\|, \|u\|) > 1.0$ GeV^2	16184	3027
$0 < M^2_{\text{rec}} < 1.1$ GeV$^2/c^4$	3916	789
$0.5 < M^2_{\text{miss}} < 1.5$ GeV$^2/c^4$	1756	299
$\|p_{\text{miss}}\| > 0.4$ GeV$/c$	495	101
$\alpha_m < 0.85$	**92**	**14**

Table 1: Table of sequential cuts for selecting SRC pn and pp pairs in the reactions ^{12}C$(p,2p)^{10}$B and ^{12}C$(p,2p)^{10}$Be.

was predicted [8, 9, 10] to allow its distribution to be assumed as independent functions of the relative and central motion of the pair, without correlation between them. Such factorization greatly simplifies SRC calculations and should be evident experimentally by the absence of correlation between the relative and central momenta of the pair, which has been verified, see Figures 10b and 10d, where the relative momentum was calculated using the formula $p_{rel} = (p_{miss} - p_{rec})/2$.

4 Conclusion

In this preliminary analysis we identified about 92 pn and 14 pp SRC candidate pairs. The observed angular correlations confirm the expected SRC signatures, indicating that the applied selection criteria are reliable. Further studies and simulations are required for final quantitative conclusions.

In the next phase of the project, I will continue working with the group on SRC analysis. Planned steps include developing a theoretical event generator for SRC processes, conducting special simulations, and applying them for more accurate event selection. At the same time, I am working on the time correction of scintillation counters located along the beam to the target. These tasks will be a continuation of the current work after the completion of the START program.

5 Addendum

Vertex cut For the reconstructed interaction vertex we required the condition

$$-589.2 < \text{Vert\_Z} < -559.2,$$

which corresponds to a 30 cm interval along the beam axis, matching the full length of the hydrogen target. Additionally, the transverse coordinates of the vertex were required to satisfy the elliptical condition

$$(\text{Vert\_X} - 0.5)^2 + (\text{Vert\_Y})^2 < 9,$$

with the further constraint $|\text{Vert\_X}| > 0$ and $|\text{Vert\_Y}| > 0$. These requirements are illustrated in Fig. 11.

Selection of (p,2p) quasi–free–scattering events. To isolate $(p, 2p)$ events from quasi–free scattering, we reject other tracks originating from inelastic reactions, predominantly pions. The basic selection is a cut on the velocities of the two measured particles. In the analysis, each of the two particles registered in the arm detectors is required to satisfy $\beta < 0.98$ and $\min\big(|t|, |u|\big) > 1$ (where t and u are the Mandelstam invariants, in GeV^2); these two requirements suppress fast and slow pions, respectively. In Fig. 12a, the cut $\beta < 0.98$ is indicated by the red lines; the suppression of small β is implemented via $\min\big(|t|, |u|\big) > 1$, which corresponds to the lower boundaries in β_L and β_R in the same panel. The threshold on $\min\big(|t|, |u|\big)$ was chosen to exclude most of the inelastic–scattering region; see Fig. 12b.

References

[1] M Patsyuk, J Kahlbow, G Laskaris, M Duer, V Lenivenko, EP Segarra, T Atovullaev, G Johansson, T Aumann, A Corsi, et al. “Unperturbed inverse

kinematics nucleon knockout measurements with a carbon beam." In: *Nature Physics* 17.6 (2021), pp. 693–699.

[2] NN Agapov, YT Borzunov, AV Konstantinov, DI Klimanskiy, IA Arkharov, ES Navasardyan, and AM Arkharov. "Cryogenic targets of the lightest gases (hydrogen, deuterium and helium-4) with GM cryocooler for experiments of high energy physics." In: *Refrigeration Science and Technology*. 2019, pp. 38–44.

[3] VA Matveev, RM Muradyan, and AN Tavhelidze. "The automodel behavior in elastic scattering at large angles and the structure of hadrons." In: *Lett. Nuovo C* 7 (1973), p. 15.

[4] "Probing high-momentum protons and neutrons in neutron-rich nuclei." In: *Nature* 560.7720 (2018), pp. 617–621.

[5] A Galavanov, M Kapishin, V Karjavine, S Khabarov, Y Kirushin, E Kulish, N Kuzmin, V Lenivenko, A Makankin, A Maksymchuk, et al. "Status of the GEM/CSC tracking system of the BM@ N experiment." In: *Journal of Instrumentation* 15.09 (2020), p. C09038.

[6] Th Blaich, Th W Elze, H Emling, H Freiesleben, K Grimm, W Henning, R Holzmann, G Ickert, JG Keller, H Klingler, et al. "A large area detector for high-energy neutrons." In: *Nuclear Instruments and Methods in Physics Research Section A: Accelerators, Spectrometers, Detectors and Associated Equipment* 314.1 (1992), pp. 136–154.

[7] Or Hen, Gerald A Miller, Eli Piasetzky, and Lawrence B Weinstein. "Nucleon-nucleon correlations, short-lived excitations, and the quarks within." In: *Reviews of Modern Physics* 89.4 (2017), p. 045002.

[8] Claudio Ciofi degli Atti. "In-medium short-range dynamics of nucleons: Recent theoretical and experimental advances." In: *Physics Reports* 590 (2015), pp. 1–85.

[9] Reynier Cruz-Torres, D Lonardoni, R Weiss, N Barnea, DW Higinbotham, E Piasetzky, A Schmidt, LB Weinstein, RB Wiringa, and O Hen. "Scale and scheme independence and position-momentum equivalence of nuclear short-range correlations." In: *arXiv preprint arXiv:1907.03658* (2019).

[10] Jiunn-Wei Chen, William Detmold, Joel E Lynn, and Achim Schwenk. "Short-range correlations and the EMC effect in effective field theory." In: *Physical Review Letters* 119.26 (2017), p. 262502.

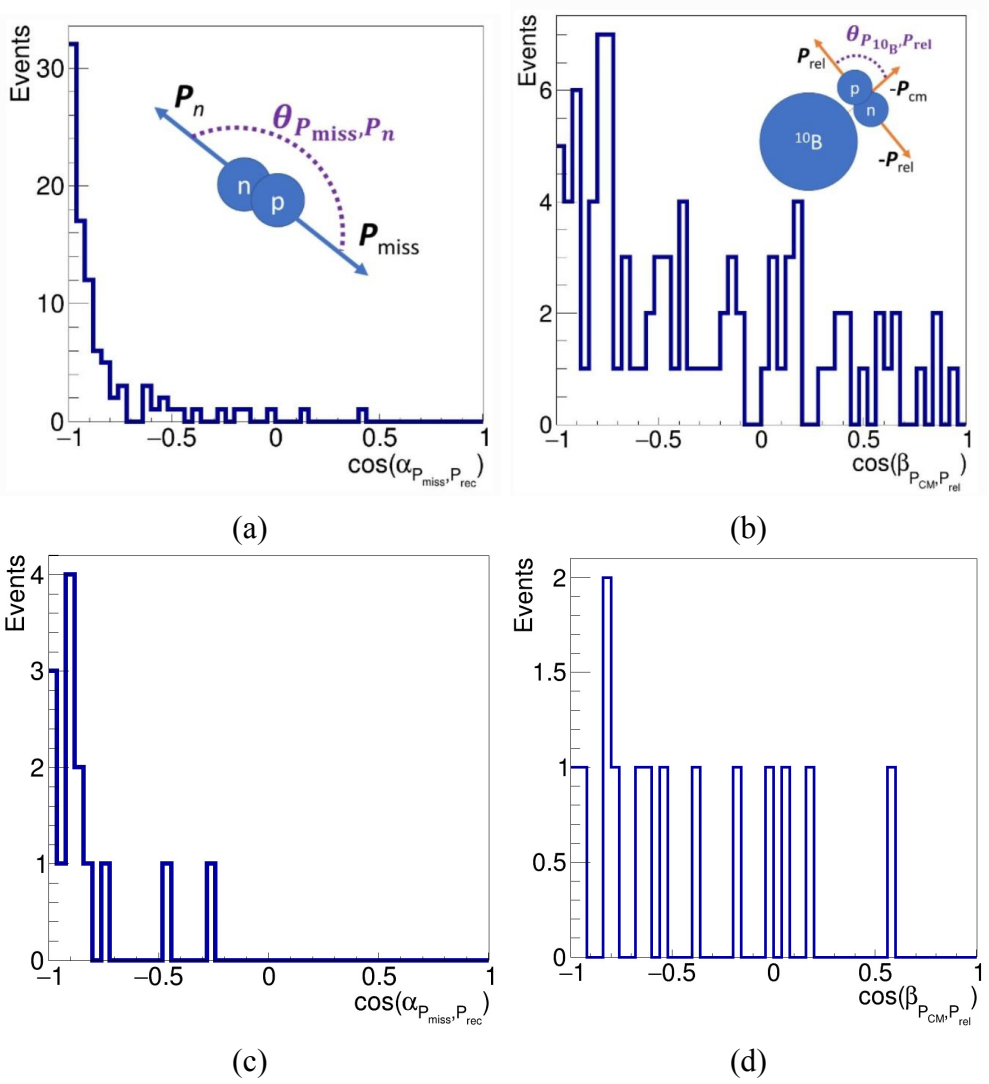

Figure 10: **Angular correlations in SRC decay events.** Distributions of the cosine of the angle between (a), (c) the recoil nucleon and the missing momentum and (b), (d) the 10B and 10Be fragments and the pair of relative momenta. (a), (b) correspond to reaction $^{12}\mathrm{C}(p,2p)^{10}\mathrm{B}$, and (c), (d) correspond to reaction $^{12}\mathrm{C}(p,2p)^{10}\mathrm{Be}$.

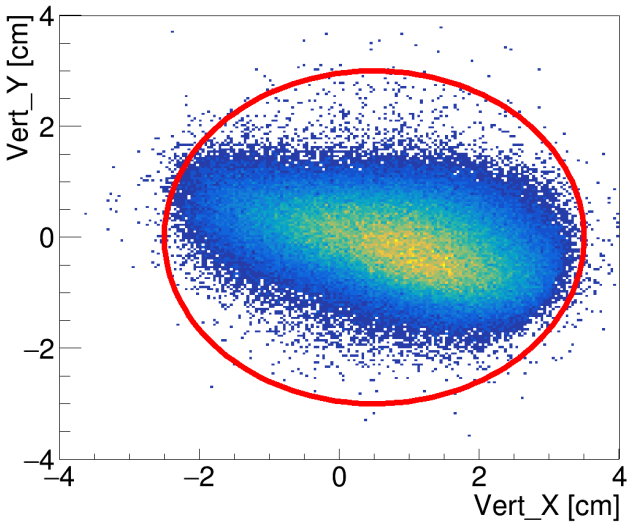

Figure 11: Reconstructed interaction vertex distribution in the transverse plane with applied elliptical cut - red line

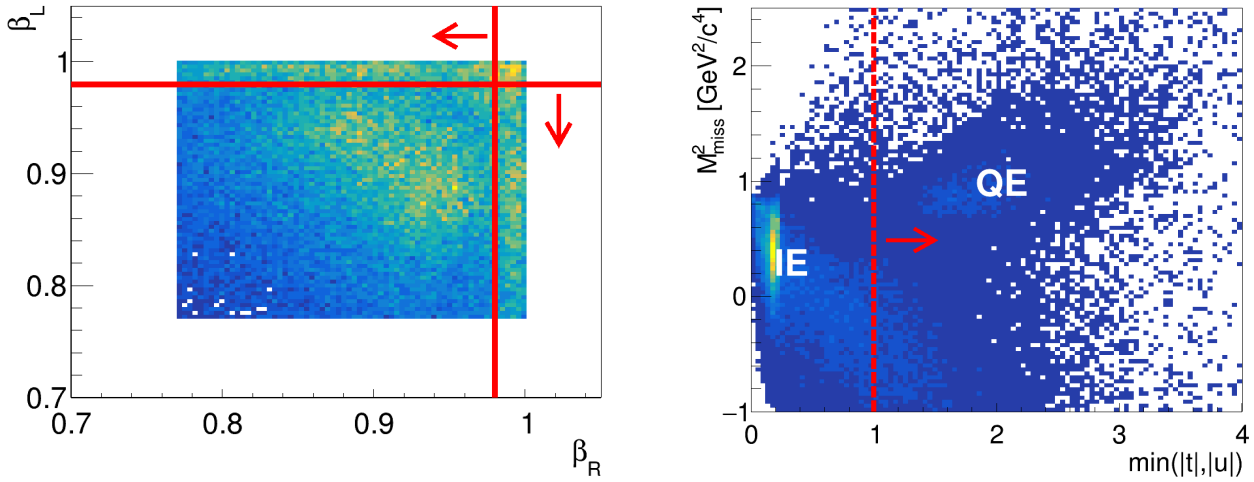

(a) Velocity cut $\beta < 0.98$ (red lines).

(b) Region excluded by $\min(|t|, |u|) > 1$.

Figure 12: Event–selection cuts in the $(p, 2p)$ analysis: (a) upper cut on particle velocities; (b) down cut on particle velocities using the Mandelstam–invariants t, u.